Journal of Hydrology 572 (2019) 169–178

Contents lists available at ScienceDirect

Journal of Hydrology

journal homepage: www.elsevier.com/locate/jhydrol

Research papers

Tree-ring reconstruction of Lhasa River streamflow reveals 472 years of hydrologic change on southern Tibetan Plateau

Feng Chen[a,b,*], Huaming Shang[b], Irina P. Panyushkina[c], David M. Meko[c], Shulong Yu[b], Yujiang Yuan[b], Fahu Chen[d]

[a] Yunnan Key Laboratory of International Rivers and Transboundary Eco-Security, Institute of International Rivers and Eco-Security, Yunnan University, Kunming, China
[b] Key Laboratory of Tree-ring Physical and Chemical Research of China Meteorological Administration/ Xinjiang Laboratory of Tree-ring Ecology, Institute of Desert Meteorology, China Meteorological Administration, Urumqi, China
[c] Laboratory of Tree-Ring Research, University of Arizona, Tucson, AZ, USA
[d] Institute of Tibetan Plateau Research, Chinese Academy of Sciences (CAS), Beijing, China

ARTICLE INFO

This manuscript was handled by Dr. Marco Borga, Editor-in-Chief, with the assistance of Di Long, Associate Editor

Keywords:
Southern Tibetan Plateau
Lhasa River
Juniper tree rings
Streamflow reconstruction
El Niño-Southern oscillation

ABSTRACT

The Lhasa River is the largest tributary of the Yarlung Zangbo River, provides up to 85% of the water supply for the city of Lhasa, and has a high ecologic and economic importance. Annual streamflow of the Lhasa River is reconstructed from *Juniperus tibetica* tree rings. The streamflow reconstruction developed for the southern Tibetan Plateau goes back to 1546 CE and has a R^2 of 0.485. Spectral and wavelet analysis indicates the existence of decadal (34 and 16 years) and interannual (8.1, 5.7, 4.8, 3.8, 3.5, 3.2, 2.7, 2.3 and 2.1 years) cycles that may reflect climate forcings. Lhasa River streamflow is significantly correlated with precipitation over a vast part of the Yarlung Zangbo River basin, and represents streamflow of the upper Yarlung Zangbo River to a certain extent. Lhasa River variation is linked with large-scale climate circulation features, such as the El Niño-Southern Oscillation (ENSO) and Asian summer monsoon. Some years of abnormally high and low streamflow are related to ENSO events. Based on the reconstruction, the probability that annual streamflow does not exceed a target defined as the instrumental-period mean was lower (48% non-exceedance probability) than during the instrumental period. This study indicates that the instrumental record does not contain the full range of streamflow, especially the lowest streamflow events, and the reconstruction makes up for this shortcoming. Future water resource supply planning based on the instrumental record and streamflow reconstructions will be able to effectively reduce the risks posed by climate change.

1. Introduction

As the source region of large Southeast and South Asian rivers, such as the Brahmaputra, Mekong and Salween, the southern Tibetan Plateau (TP) has important influence on Asian hydrology (Bolch et al., 2012; Yao et al., 2012; Fan and He, 2015), and its river systems affect more than 3 billion people. The hydrological regime on the TP is dominated by glacier melt, snow meltwater, and/or summer precipitation. High flows in August are the result of warm summer temperature and monsoon precipitation. Streamflow data from hydrological stations located upstream of transboundary rivers at the TP show an increasing trend with the accelerated melting of glaciers since at least 1980 (Li et al., 2014; Fan and He, 2015). Due to fast growing demands on water resources for drinking water, tourism and hydropower generation in recent decades, the supply of water from the TP as one of the main limitations to sustainable development of countries in downstream regions has been widely documented (Jacobs, 2002; Xue and Wang, 2005; Immerzeel et al., 2010; Gain and Wada, 2014; Orr et al., 2012). Due to uneven distribution of monsoonal rainfall, this applies even to downstream regions with high annual precipitation, such as Vietnam, Thailand, India (Kumar et al., 2005; Li et al., 2011b; Trinh et al., 2013). To improve water resource planning with the ultimate goal of improving peoples' lives it is important to carry out scientific research on the spatiotemporal streamflow variation of various rivers of the TP. Continuous hydrological observations on the TP are not available before 1950, thus providing poor temporal and spatial coverage. The application of remote sensing techniques and hydrological models has greatly improved the spatial coverage of

* Corresponding author at: Yunnan Key Laboratory of International Rivers and Transboundary Eco-Security, Institute of International Rivers and Eco–security, Yunnan University, Kunming, China.
E-mail address: feng653@163.com (F. Chen).

https://doi.org/10.1016/j.jhydrol.2019.02.054
Received 5 December 2018; Received in revised form 6 February 2019; Accepted 14 February 2019
Available online 02 March 2019

hydrological data (Chen et al., 2017; Long et al., 2016, 2017; Yi et al., 2017; Huang et al., 2018a, b; Huang et al., 2018c). However, long-term streamflow analysis is still limited by a lack of long-term and high-resolution hydrological records on the TP.

Moisture-sensitive tree ring width data provide continuous, high-resolution hydroclimatic records for several centuries or even millennia (Fritts, 1976; Meko et al., 2012; Harley et al., 2017; Stagge et al., 2018; Tamkevičiūtė et al., 2018). Long-term streamflow series can be constructed by correlating tree-ring series with observed streamflow, and the characteristics of the resulting streamflow reconstruction can be analyzed at different time scales for better understanding of fluctuations and trends in the water resource. Many streamflow reconstructions have been developed in North and South America (e.g., Meko and Woodhouse, 2005; Lara et al., 2008, 2015; Maxwell et al., 2011; Urrutia et al., 2011; Woodhouse et al., 2012; Mundo et al., 2012; Ferrero et al., 2015; Coulthard et al., 2016; Muñoz et al., 2016; Fernández et al., 2018). A spatial streamflow reconstruction for the US has been developed from a continental tree-ring network (Ho et al. 2017). Streamflow reconstructions also have been carried out for Asia, including the TP (e.g., Agafonov et al., 2016; D'Arrigo et al., 2011; Cook et al., 2013; Davi et al., 2013; Gou et al., 2007; Liu et al., 2010; Panyushkina et al., 2018; Yang et al., 2012). The number of available streamflow reconstructions for the TP is much lower than for South and North America. Despite the potential of juniper tree rings (*Sabina tibetica* Kom.) for hydroclimatic reconstructions (Liu et al., 2011; He et al., 2013; Zhang et al., 2015), the southern TP remains largely unexplored.

The aim of this research is to show a tree-ring based streamflow reconstruction for the Lhasa River in the Yarlung Zangbo River Basin for the last 472 years. We analyze characteristics of the streamflow reconstruction and its spatial representation over the TP. Finally, to identify the main climatic forcings affecting Lhasa River streamflow, we compare the Lhasa River reconstruction with atmospheric circulation indices such as sea surface temperatures (SST) of the Indo-Pacific Oceans and El Niño- Southern Oscillation (ENSO). We believe this is the first research to attempt to use tree-ring width for streamflow reconstruction on the southern TP.

2. Materials and methods

2.1. Geographical settings

The Lhasa River, the largest tributary of the Yarlung Zangbo River, originates on the southern slopes of the Nyenchen Tanglha Mountains (Fig. 1). The Lhasa River provides most of the water supply for Lhasa, the largest city in Tibet. The Lhasa River lies between 90°05′ E and 93°20′E longitudes and 29°20′ E and 31°15′N latitudes, and drains a watershed of 32,558 km^2. Natural streamflow of the Lhasa River is supplied mainly by precipitation, groundwater and glacier melt water, accounted for 46%, 28% and 26% of the total streamflow (Liu, 1999), respectively. The catchment area above the Lhasa hydrological station is 26,225 km^2, and accounts for 80.5% of the total basin area (Lin et al., 2008). Annual streamflow of the Lhasa River averaged 295 m^3/s during the period 1956–2017. Due to the influence of glacier melt water and the summer monsoon, the main streamflow peaks occur in summer (August, 876 m^3/s). The lowest streamflow occurs in winter (March, 49.4 m^3/s).

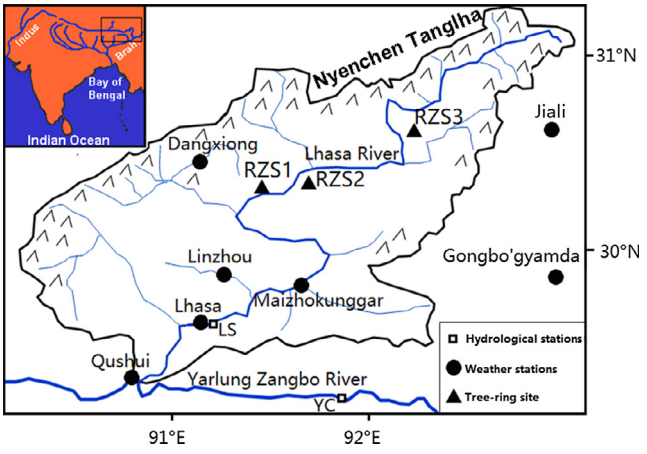

Fig. 1. Map showing the Lhasa River Basin and location of the sampled sites, weather and hydrological stations. Names of the site and stations are listed in Table 1.

The climate in the headwaters of the Lhasa River is classified as continental plateau semi-arid with summer monsoonal influence and strong ultraviolet radiation. For the period 1963–2017, average annual temperature is 1.9 °C, the warmest month is July (11.1 °C) and the coldest month is January (−9.0 °C). Average annual precipitation is 473.8 mm, and July (124.3 mm) is the wettest month (Fig. 2A). The basin is covered mostly by grassland and our sampling site, a juniper forest, stands on a southeastern facing slope characterized by thin and rocky soil, favoring a strong influence of hydroclimatic variation on tree growth.

2.2. Tree-ring data

The long-lived, undamaged juniper trees (*Juniperus tibetica* Kom.) at Tanggu town, near the Lhasa River valley, were sampled from open stands with shallow or rocky soils (Table 1). At least two cores were taken from live trees with the 5.1 mm diameter Swedish increment borer in the RZS1 site in 2007, and one core per tree was collected from live trees with the 10.0 mm diameter Swedish increment borer in the RZS2 and RZS3 site in 2018. In combination, the three sites provide 85 cores taken from 63 trees. All tree-ring cores were air-dried, glued to wooden holders, and fine-polished with 400-grit sandpaper.

Ring widths were measured to an accuracy of 0.001 mm using a TA Unislide Measurement System. Tree-ring width data were crossdated by visual pattern matching, and crossdating was checked using COFECHA software (Holmes, 1983). To remove non-climatic trends while preserving the low-frequency climate signal, ring-width series were detrended and converted to core indices with a negative exponential function. These indices were combined into a final regional standard (STD) chronology based on the bi-weight robust mean as implemented in ARSTAN software (Cook, 1985). The period of usable chronology–represented by adequate sample depth–was evaluated with the expressed population signal (EPS, Wigley et al., 1984). The EPS is a function of the mean series intercorrelation, which is the mean correlation between individual ring-width series and number of cores.

2.3. Hydroclimatic data and statistical methods

Local monthly meteorological data from the Danxiong station was used in this research. The station is located at 91.06°E, 30.29°N, 4200 m *a.s.l.* and its records date from 1963 to 2017. Climagrams show a strongly continental climate, with precipitation peaking in July (Fig. 2A). Lhasa River streamflow data, 1956–2017, were obtained for the Lhasa hydrological station (LS), located at 91.15°E, 29.64°N, 3670 m a.s.l. No reservoirs are upstream of LS, and therefore this record approximately reflects the natural flow variation of the Lhasa River. The annual (calendar year) streamflow of the Lhasa River at LS correlates strongly ($r = 0.84$, $P < 0.01$) with annual streamflow of the Yarlung Zangbo River at the Yangcun hydrological station (YC, 91.82°E, 29.26°N, 3550 m a.s.l) for the 1960–2009 period of overlap of the two records (Fig. 2C).

To reveal the linkages between climate, streamflow and tree-ring data, we calculate correlations between tree-ring width series and various monthly combinations of station hydroclimatic data. A reconstruction model was estimated by simple linear regression of the

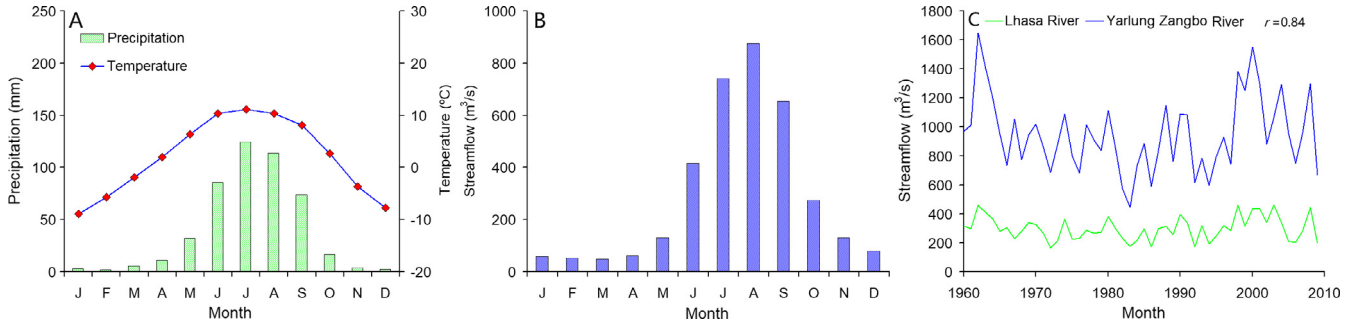

Fig. 2. Historical data on climate and hydrology of the study basin. (A) Monthly mean precipitation and temperature from the Dangxiong weather station. (B) Monthly mean streamflow from the Lhasa hydrological station. (C) Time series of gauged annual streamflow of Yarlung Zangbo River and Lhasa River.

water year (August–July) streamflow series on the standard tree-ring chronology. We assessed the reliability of the reconstruction model applying leave-one-out cross-validation method (Michaelsen, 1987). The quality of the streamflow reconstruction equation was measured using the Pearson correlation coefficient (r), product mean test (PMT), the sign test, the reduction of error (RE) and coefficient of efficiency (CE) (Fritts, 1976; Cook and Kairiukstis, 1990).

A 20-year low-pass filter was applied to the streamflow reconstruction to identify extended ($\geq$10 years) periods of high- and low-streamflow before the instrumental period. Thresholds of $\pm$ 2σ from the long-term mean were used classify extremely high and low streamflow years. Spectral analysis by the wavelet analysis (Torrence and Compo, 1998) and multi-taper method (MTM; Mann and Lees, 1996) were used to reveal the cyclic characteristics of reconstructed streamflow. The Morlet wavelet with parameter m = 6 was used in the wavelet analysis. A 5 × 3 π taper was used in the MTM analysis, and the power was tested against a red noise process at the 0.05 significance level. To show that our reconstruction represents large-scale hydroclimatic variability, we calculated the Pearson correlation coefficient of that series with the streamflow record of the Yarlung Zangbo River and CRU gridded precipitation (Harris et al., 2014).

To reveal linkages with the atmospheric circulations, composites of August–July SST and June–August (monsoon season) 850 hPa vector wind anomalies from the mean were created for the lowest and highest streamflow years (n = 10) during the period 1948–2017. Furthermore, the correlation coefficients between the Lhasa River streamflow and atmospheric circulation indices were assessed to identify the main climatic forcings affecting interannual changes in streamflow. To further analyze the influence of El Niño events, we used the superposed epoch analysis (SEA, Haurwitz and Brier, 1981) and the ENSO index (Li et al., 2011a) to evaluate significance of relationships in the presence of autocorrelation. Finally, to assess whether the probability of meeting this minimum flow differed between the instrumental period and prior periods we used the cumulative distribution function (CDF) of reconstructed mean annual streamflow. Using the lognormal CDF we compared the specific probabilities of not meeting normal river streamflow targets (in our case, 358.8 m^3/s) between the reconstructed instrumental period (1956–2017) and (1) the full reconstructed period and (2) pre-instrumental periods equal in length to the gaged record (n = 61 years).

3. Results

3.1. Tree-ring regional chronology

The resulting regional chronology covers the period 1211–2017 CE. The tree-ring chronology for use in reconstruction was truncated at 1546 CE, before which the EPS value drops below 0.85. The strength of the common signal can be assessed using the mean correlation of the individual ring-width series (with master). As the three sampling sites were very close (mean distance among the three sites is about 20 km), the individual ring-width series from the three sites showed a common signal (r = 0.620), and reflected the common responses to hydroclimatic influences. Consequently we combined all individual ring-width series into a regional chronology. The regional chronology had high standard deviation, signal-to-noise ratio, variance in first eigenvector and expressed population signal, and also revealing that the radial growth of juniper trees was responding to common factors (Table 2).

3.2. Development of steamflow reconstruction

The chronology is more strongly correlated with precipitation than with temperature (Fig. 3). Significant ($p < 0.05$) correlation with temperature occurs in previous July ($r = -0.31$) and current May ($r = -0.57$) and June ($r = -0.41$). Correlation of the chronology with monthly precipitation is significant ($P > 0.05$) from May through June of the current year and from July to September of the previous year (Fig. 3). Highest monthly precipitation correlation (r = 0.60) is reached in current May. The significant correlation with monsoon precipitation of the previous season could be explained by positively autocorrelated growth. Good growth conditions in one year leave the tree better prepared to start growth next year. Much higher positive correlations were seen between tree rings and streamflow from previous July to current March (r = 0.45–0.68). High monthly streamflow correlation (r = 0.63 and 0.42) is found in current June and July during the monsoon season. Correlation of tree-ring index with precipitation and streamflow is increased with aggregation of the hydrologic series over several months. The highest correlation between tree-ring series and seasonalized precipitation and streamflow was found for total August–June precipitation (r = 0.706, $p < 0.001$) and September–July streamflow (r = 0.761, $p < 0.001$) intervals. While September–July streamflow

Table 1
Location of the tree-ring site, weather station and hydrological station (see Fig. 1).

Site	Lat. (N)	Long. (E)	Elevation (m, asl)	Aspect	Slope	Cores/Trees	Species
RZS1	30.35°	91.55°	4315	SE	10–25°	44/22	*Juniperus tibetica*
RZS2	30.40°	91.70°	4290	S	15–25°	20/20	*Juniperus tibetica*
RZS3	30.70°	92.15°	4360	S	10–25°	21/21	*Juniperus tibetica*
Dangxiong	30.29°	91.06°	4200				
Lhasa	29.64°	91.15°	3670				
Yangcun	29.26°	91.82°	3550				

Table 2
Statistics of STD tree-ring width chronology used in the reconstruction.

Statistic	Value
Mean sensitivity	0.249
Standard deviation	0.293
First order autocorrelation	0.519
Mean correlation with master	0.620
Variance in first eigenvector (%)	43.7
Expressed population signal (EPS)	0.959
First year where EPS > 0.85 (number of trees)	1546 (6)

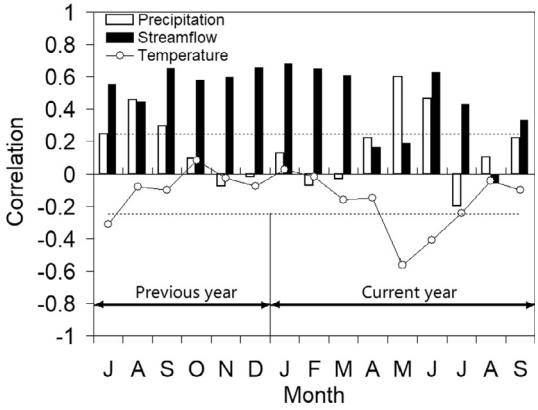

Fig. 3. Correlations of standard (STD) chronology with monthly temperature, precipitation and streamflow. Correlations with precipitation and temperature were calculated for the common period 1963–2017, while those for streamflow were calculated for 1956–2017. The dashed lines indicate the 95% confidence level for the correlation.

may be an optimum hydroclimatic target for reconstruction, the Chinese governmental stakeholders prefer a long series of streamflow for the water year (August-July, $r = 0.696$, $p < 0.001$) to implement directly into the regional water management and land use planning in the Tibet Autonomous Region. The analysis of gauge and weather observations indicates that total August–June precipitation and August–July streamflow of the Lhasa River are strongly correlated ($r = 0.846$, $p < 0.001$). To secure practical implementation of our modeled data, water year (August-July) streamflow was selected as the predictand for the reconstruction model.

A regression model was developed to reconstruct the water year flow (August-July). The reconstruction model is,

$$y = 188.545 + 173.973x$$

Where x is the standard tree-ring chronology and y is the reconstructed streamflow in m^3/s. The calibration–verification statistics indicate a reliable model (Table 3). The model has a highly significant ($p < 0.01$) overall-F and explains 48.5% ($R^2 = 0.485$) of the actual streamflow variance for the 1956–2017 calibration interval. Results of product-mean and the sign test also indicate a successful model. Positive RE and CE are positive, revealing useful skill when the model is applied to data not used in the fit. The prediction R^2, based on leave-one-out cross-validation error is only slightly lower than the calibration R^2 (45.4% vs 48.5%).

Table 3
Leave-one-out cross-validation statistics for the streamflow reconstruction of the Lhasa River based on tree rings.

r	r_{adj}^2	ST	RE/CE	PMT
0.674**	0.485	$45^+/16^{-**}$	0.454/0.446**	5.001**

r: correlation coefficient; r_{adj}^2: explained variance adjusted for degrees of freedom; RE: reduction of error; CE: coefficient of efficiency. ST: sign test. PMT: product-of-means test. **Significant at $p < 0.01$.

As shown in Fig. 4, the reconstructed streamflow closely tracks the observed streamflow at high and low frequencies, with a few exceptions. The compression of variance of the reconstruction relative to the observed streamflow is expected given that less than half the observed variance is explained in reconstruction. While our tree-ring chronology is also highly correlated with calendar-year normalized streamflow for the Yarlung Zangbo River ($r = 0.61$, $P < 0.001$) for the period 1960–2009 (Fig. 4B), we did not develop a streamflow reconstruction for that river because of its relatively large draining basin. However, the comparison result in Fig. 4B suggests that the tree-ring width variability could be also employed to model the Yarlung Zangbo flow in future.

3.3. Analysis of streamflow reconstruction for the Lhasa River

The water year (August-July) streamflow of the Lhasa River reconstructed over the last 472 years is shown in Fig. 5. Remarkable periods of low streamflow occurred in 1588–1609, 1627–1642, 1656–1679, 1733–1743, 1754–1786, 1792–1809, 1822–1845, 1874–1888, 1912–1935, 1942–1964 and 1972–1988, while high streamflow periods occurred in 1549–1587, 1610–1626, 1643–1655, 1680–1690, 1697–1732, 1744–1753, 1810–1821, 1846–1873, 1889–1911 and 1989–2007. Extreme years are listed in Table 4. As indicated by our streamflow reconstruction, the low streamflow epoch in 1874–1888 is the most severe drought with low streamflow in the study area since 1546 CE.

As shown in Fig. 6A, MTM analysis detected 34- and 16-year cycles (at 95% level) in reconstructed streamflow data for the Lhasa River. Some interannual cycles (8.1-year (95%), 5.7-year (95%), 4.8-year (95%), 3.8-year (99%), 3.5-year (99%), 3.2-year (99%), 2.7 year (95%), 2.3 year (99%) and 2.1 year (95%)) were also found. Temporal characteristic of the different cycles is showed using wavelet analysis (Torrence and Compo, 1998) (Fig. 6B). The largest significant feature in the CWT is high variance near 34 years centered in the 2nd half of the 19th Century. The time plot shows this variance as a major wave with driest conditions near 1875. Other significant patches of variance are near 16 years, centered at about 1700 and 1950. Some significant high-frequency periodicities on most of the reconstructions are found between 2 and 8 years. These findings are confirmed by the MTM spectra.

3.4. Streamflow and circulation analysis

Reconstructed Lhasa River streamflow is significantly correlated ($p < 0.001$) with August-June CRU TS 4.01 gridded ($0.5^\circ \times 0.5^\circ$) precipitation over a broad geographic region, especially in the Yarlung Zangbo River basin (Fig. 7A). The results confirm that our streamflow reconstruction captures regional hydroclimatic changes. Meanwhile, significant negative correlations are found in Pakistan and western India, with strongest correlations occurring in southern Pakistan, especially at the Arabian Sea coastline near Gwadar Port.

Strongly significant regions of SST correlation are found in the tropical Indian Ocean and western Pacific Ocean, suggesting that these tropical domains are the main moisture sources for our research area (Fig. 7B). During the highest streamflow years, the SST anomaly is negative in the tropical eastern Pacific but positive in the western Pacific Ocean, indicating a cold ENSO phase (La Niña), and vice versa (Fig. 7C, D). Highest streamflow years are characterized by strong southwesterly mean 850 hPa winds over the western TP and Pakistan (Fig. 7E). Lowest streamflow years are characterized by strong westerly winds at 850 hPa from inland over the TP (Fig. 7F).

Comparison of our reconstruction with the ENSO index developed by Li et al. (2011a) reveals no significant relationship between Lhasa river streamflow and ENSO. Superposed epoch analysis, however, shows a significant increase in streamflow during strong La Niña episode (year = 0) and low streamflow during (year = 0) and two years after (year = 2) during strong El Niño episodes (Fig. 8). The probability

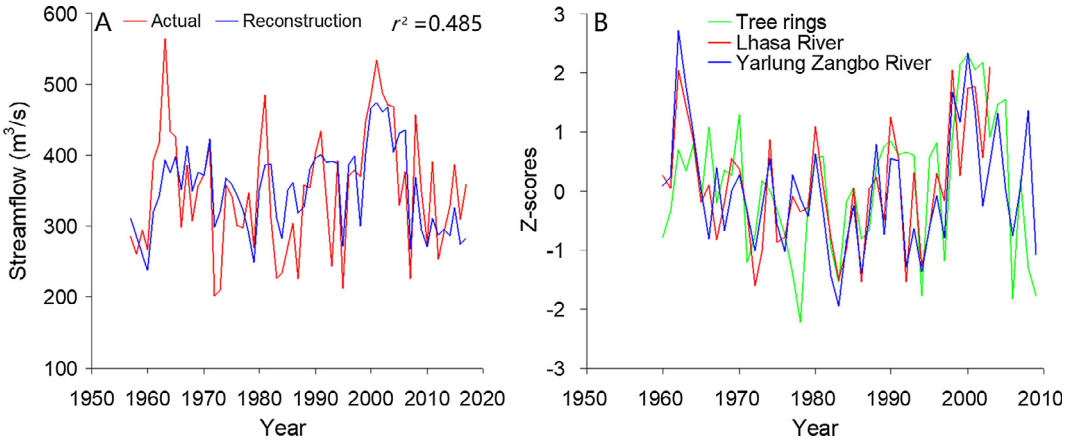

Fig. 4. Time series plots streamflow and tree-ring series for calibration period. (A) Instrumental (actual) and reconstructed streamflow, 1956–2017. (B) Z-scores of tree-ring chronology and instrumental streamflow records for Yarlung Zangbo River and Lhasa River.

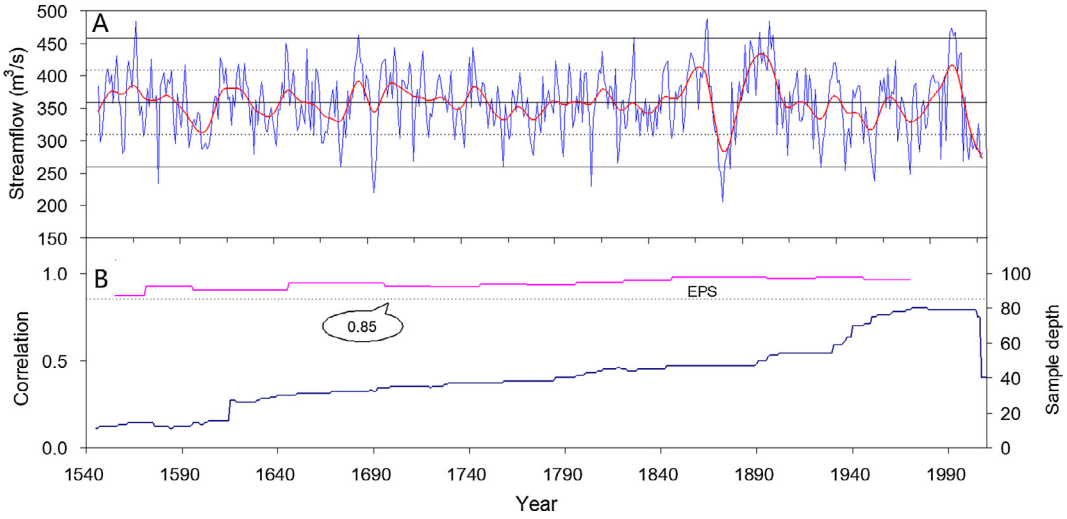

Fig. 5. Tree-ring chronology and streamflow reconstruction. (A) Reconstructed streamflow for the period 1546–2017 CE (thin line) and the 20-year low-pass filter curve (thick line). Horizontal lines show the average reconstructed streamflow (thin line in the middle), one standard deviation (dotted line) and two standard deviations, (outer lines). (B) Expressed population signal (EPS) and sample depth of standard tree-ring chronology. The dotted line denotes the 0.85 EPS criterion for signal strength acceptance (Wigley et al., 1984).

Table 4
Extreme low-flow and high-flow period in Lhasa River reconstruction from 1546 to 2017. Listed "Low" and "High" are for single years. Listed "Period" in rightmost column is the flow less than one standard deviation for more than two consecutive years.

Rank	Year	(Low)	Year	(High)	Period	Low > 2 years
1	1879	205.4	1871	487.1	1600–1604	290.7
2	1693	220.0	1904	483.8	1692–1694	245.0
3	1809	230.1	1566	483.3	1873–1883	286.7
4	1578	234.5	1870	480.0	1930–1932	285.2
5	1960	238.3	2001	473.3	1958–1960	261.0
6	1979	249.1	1899	467.1	1977–1979	286.9
7	1878	251.5	2003	466.9		
8	1944	254.5	2000	465.2		
9	1877	256.6	1685	463.6		
10	1883	256.7	1906	462.9		
11	1694	257.1	2002	461.0		
12	1692	257.8	1832	459.4		
13	1931	258.3	1894	454.7		
14	1959	260.0	1646	450.7		
15	1675	260.6	1891	447.6		

of not meeting the 358.8 m^3/s streamflow target (the mean of reconstructed streamflow) computed from CDF of the reconstructed streamflow series over the pre-instrumental period (0.48) was remarkably lower than the probability calculated for the gauged record (0.56) (Fig. 9).

4. Discussion

4.1. Dendrohydroclimate correlations

The significant positive correlation between tree-ring index and total August–June precipitation indicated that the water-deficit stress was a major limiting factor for the radial growth of juniper trees. Like the tree-ring record, total August–June precipitation strongly correlate to streamflow variations, indicating that corresponding signals from both climate parameters were contained within the tree-ring record and streamflow. The strong correlative linkage between tree growth and streamflow supports this conclusion. In the Lhasa River basin, dry conditions before the onset of the summer monsoon cause drought stress to the juniper trees and are thus limiting the radial growth of juniper trees. Thus, tree growth and riverflow benefit from the former summer and current spring-early summer precipitation, which increase the soil moisture content during the early part of the growing season.

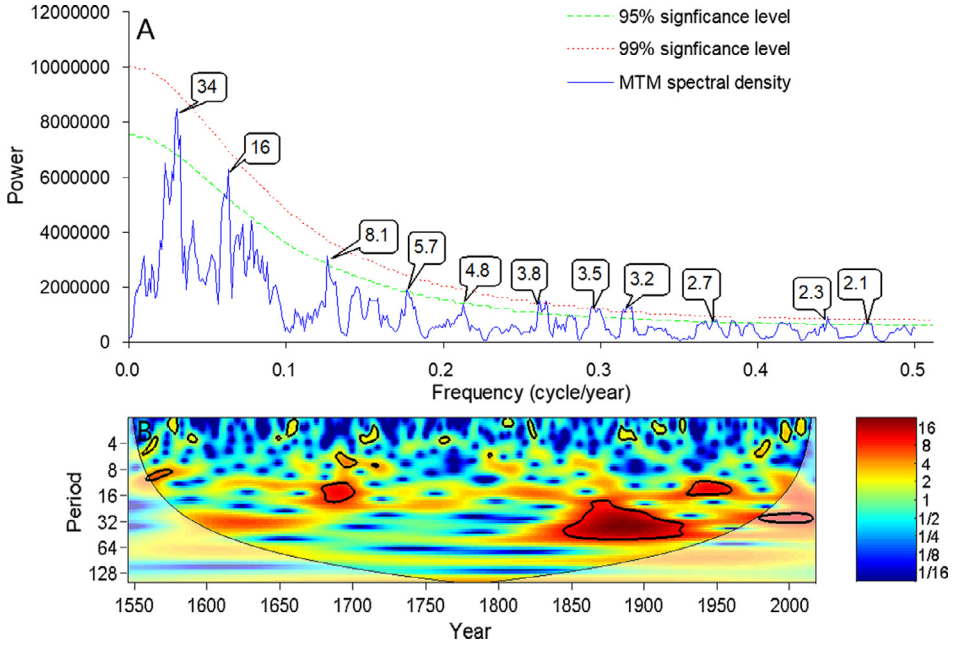

Fig. 6. Spectrum and wavelet analysis of Lhasa River reconstruction. (A) Multitaper method (MTM) spectral density of the reconstructed Lhasa River streamflow. The dashed and dotted lines indicate the 95 and 99% confidence, respectively. (B) Continuous wavelet transform (CWT) and smoothed time plot of reconstruction, 1546–2004. Red line on y-axis of CWT shows wavelength-range emphasized by the filtered series in C. The CWT shows color-coded variance as a function of frequency and time. High variance is red and low variance is blue. Variance significant relative to red noise is outlined in a black line. (For interpretation of the references to color in this figure legend, the reader is referred to the web version of this article.)

Most of the correlations between the radial growth of juniper trees and spring temperature were negative. High May–June temperatures enhance evapotranspiration and thus decrease soil moisture availability and streamflow. Thus, a year with above average spring temperature is also indicative of both decreased streamflow and depressed ring growth.

4.2. Lhasa River streamflow and climatic forcings

The Lhasa River basin, located on the monsoonal Tibet, is affected by large-scale ocean–atmosphere–land circulation systems (Zhang et al., 2007; Gao et al., 2017). Results of superposed epoch analysis also show that strong El Niño events correspond to low river discharge on the TP (Fig. 8B). A good example would be the strong 1877–1878 El Niño and the low streamflow period of 1874–1888. Instrumental, historical and various other climate proxies show widespread dry conditions in 1877–1878, especially in Asia and South America (Aceituno et al. 2009; Hao et al., 2010, Cook et al., 2010, 2013). Composite maps of the ten highest and lowest streamflow years show that abnormally low and high streamflow corresponds with ENSO events, pointing to ENSO as a causal mechanism for streamflow variation in Tibet, China (Fig. 7C, D). The frequency cycles of reconstructed series (34-year, 8.1-year, 5.7-year, 4.8-year, 3.8-year, 3.5-year, 3.2-year, 2.7 year, 2.3 year and 2.1 year) are also similar to the ENSO cycles (Li et al., 2011a). These results resemble other findings in nearby areas and suggest the impact of SST in the tropical oceans on streamflow in Tibet (Shrestha and Kostaschuk, 2005; Zhang et al., 2007). As shown by Gao et al. (2017), variations of oxygen isotopic composition precipitation in the Lhasa basin of southern Tibet is mainly influenced by ENSO-induced anomalies in southwesterly water vapor flux that originates from the Bay of Bengal, Arabian Sea and tropical Indian Ocean. During cold ENSO events (La Nina), enhanced southwesterly and southerly winds bring abundant moisture across the Indian Peninsula. This moisture travels northward, causing increased rain over southern Tibet, and results in lower $\delta^{18}O_p$ at Lhasa, and vice versa (Zhou et al., 2001; Yao et al., 2013; Gao et al., 2017; Fig. 7). Our results indicate that Lhasa River streamflow is highly positively correlated with the regional precipitation variation. It is thus not surprising that our streamflow reconstruction also displays fingerprints of ENSO events.

Meanwhile, our results also indicate that SSTs in the tropical Indian Ocean are negative correlated with Lhasa River streamflow, suggesting ENSO is not the only forcing of Lhasa River streamflow variations; there might also be linkages with tropical and North Indian climate change. The highest streamflow values were also associated with unusually cool SSTs in the Indo-Pacific Ocean (Fig. 7C). A previous study has revealed that cold (warm) spring-summer SSTs over the equatorial Western Indian Ocean tend to concomitant with strong (weak) southwesterly monsoon (Jia and Zhou, 2003). During highest streamflow years (cold SSTs), strong southwesterly flow at 850 hPa occurs over western Tibet and Pakistan (Fig. 7F). This strong phase of southwesterly monsoon should advect water vapor from the Arabian Sea, and lead to increased precipitation and runoff. During lowest streamflow years, the opposite pattern occurs. These results together reveal that the tropical Indian Ocean – especially the Arabian Sea – is an important water vapor source for southern Tibet, and that colder SSTs in the Arabian Sea tend to increase northward water vapor transport to the southern Tibet and likely contribute to increase streamflow in that region.

4.3. Water management implications

The 472-year reconstruction presented in this paper, the first streamflow reconstruction for the southern TP from tree rings, is also highly correlated with streamflow of the Yarlung Zangbo River. This spatial representation is especially important for understanding the long-term water resource variation in the southern TP, where environmental protection is a priority and the water resource is fundamental for sustainable development and economic activities such as agriculture, hydroelectric power generation, and tourism. The Lhasa River provide up to 85% of the water supply for the Lhasa city, which is the biggest city in Tibet autonomous region.

The pronounced continuous multi-year decline in average streamflow over 1874–1888 highlights the vulnerability of the water resource supply for Lhasa city. A return of severe large-scale drought to the southern TP would endanger sustainable water resources management of the Yarlung Zangbo River basin, and have important implications for downstream plains regions in Bangladesh and India. A potential limitation depends on the frequency and severity of large-scale drought in the southern TP. Although water resource allocation in the southern TP is less than the estimated reliable diversion yield, these values were based on the instrumental streamflow record. In addition to the Yarlung Zangbo River, many other large Asian rivers flow through the southern TP and often experience similar precipitation/drought variation from

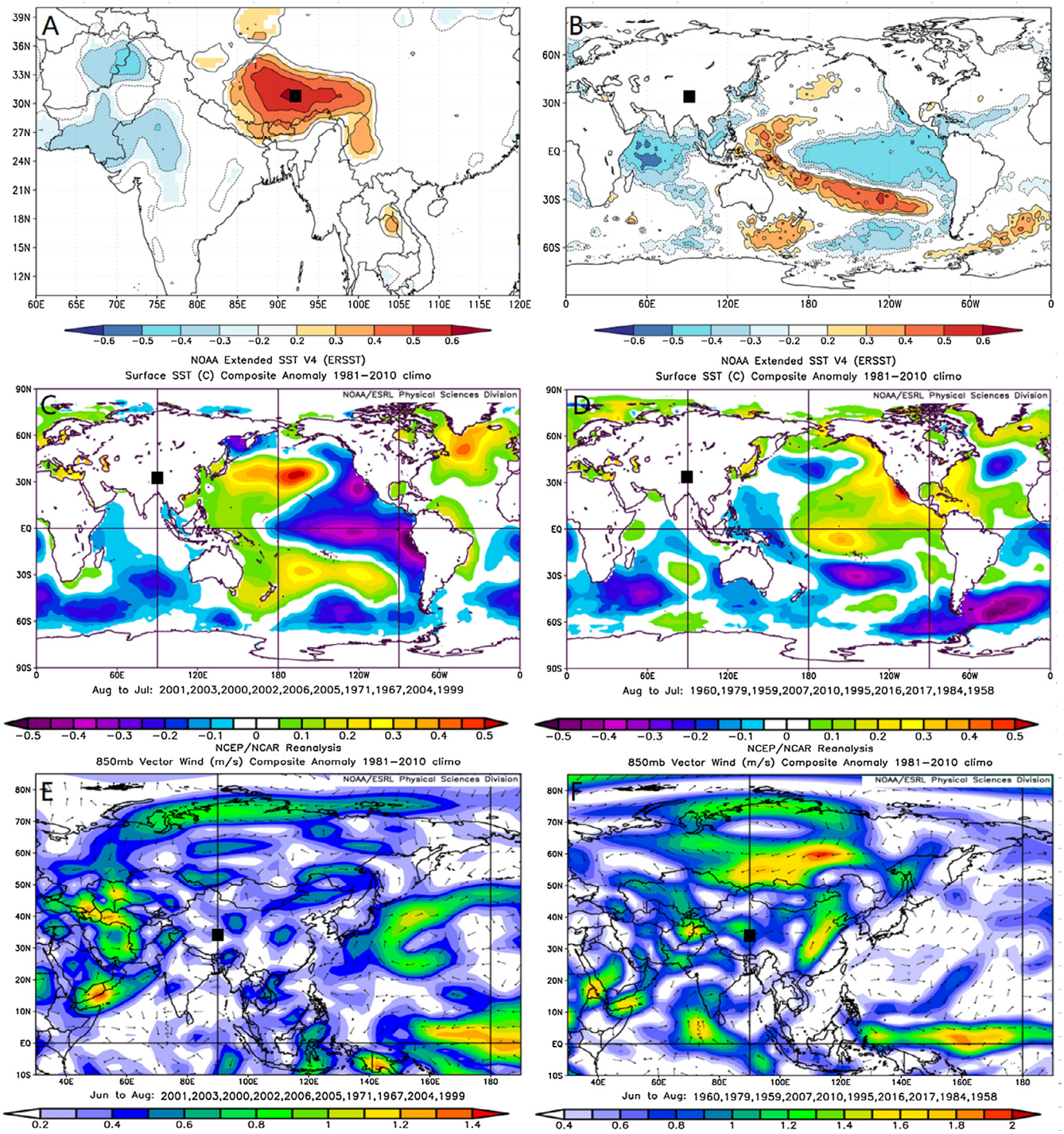

Fig. 7. Spatial correlation fields illustrating large-scale climatological linkages of reconstructed Lhasa River streamflow. (A) Spatial correlation fields of reconstruction with regional gridded precipitation for the period 1956–2016. (B) Correlation patterns of the reconstruction with August –July SST over the common period 1948–2017. Correlations were calculated after removing the linear trends of data. (C) Composite anomaly map of August–July SST for the 10 highest streamflow years. (D) Composite anomaly map of August –July SST for the 10 lowest streamflow years. (E) Composite map of 850-hPa vector wind (June-August) for the 10 highest streamflow years. (F) Composite map of 850-hPa vector wind (June-August) for the 10 lowest streamflow years. Analysis period for maps in C-F is 1948–2017. Our study area is indicated by filled square.

the Asian summer monsoon that influences the vital spring-summer runoff and snow coverage (Liu et al., 2011; Gou et al., 2013; He et al., 2013, 2018; Chen et al., 2018). Large-scale drought on the TP has been reported in tree-ring based drought reconstructions at multiple forest sites across the TP at various times, including the 1870 s and 1920 s (Brauning and Griebinger, 2006; Sano et al., 2012; Cook et al., 2013; Yang et al., 2014; Zhang et al., 2015). The Monsoon Asia Drought Atlas (MADA) offers support for extensive regional drought over the TP in only a few of the years over 1874–1888, but the MADA reconstructions are not validated in our region (Cook et al., 2010). It is worth noting that other moisture proxies from tree rings show a much smaller magnitude of this particular regional drought than our reconstruction. Our series suggests a nearly 30% reduction of Lhasa streamflow in 1876–1882. Overall, this extraordinary episode of low flow in the

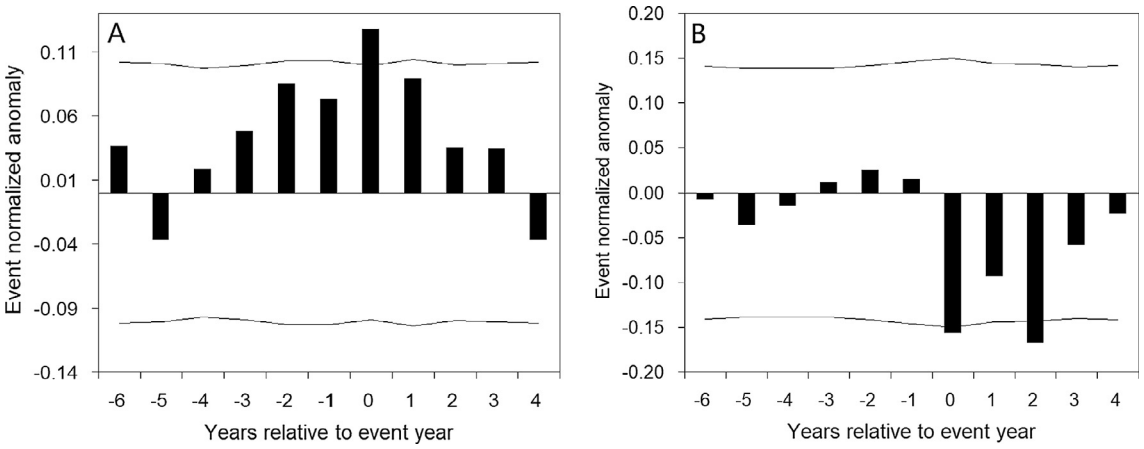

Fig. 8. Superposed epoch analysis (SEA) of the impact of 30 strong La Niña (A) and El Niño (B) events on Lhasa River streamflow reconstruction.

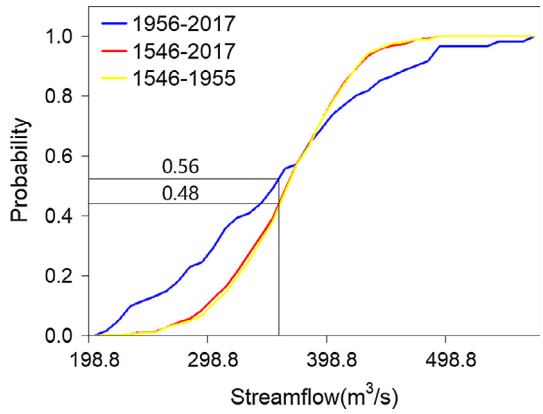

Fig. 9. Cumulative distribution functions (CDFs) of instrumental and reconstructed annual streamflow. Plots shown for different sub-periods: instrumental (1956–2017), full-length (1546–2017), and pre-instrumental (1546–1955). Annotated are empirical non-exceedance probabilities, or the probabilities of not exceeding 358.8 m^3/s, which is the long-term instrumental mean.

reconstructed series needs to be investigated further with additional collections of moisture sensitive tree-ring sites from critical runoff-producing regions of the Lhasa and Yarlung Zangbo Rivers.

Water resources management is often based on the extreme streamflow values in instrumental records. Reconstructed streamflow may provide additional information about the probability distributions of streamflow during pre-instrumental period, and this information can contribute to water resource allocation planning. During the pre-instrumental period there was a drop to a 8% lower chance that annual streamflow would not meet this target. But this does not mean we can let down our guard against extreme drought events. If the water supply is insufficient for normal river streamflow targets (in our case, 358.8 m^3/s) in the southern TP for consecutive years, impacts could be huge downstream in India and Bangladesh. For example, the reconstructed dry episodes (Table 3) suggest that annual streamflow of the Yarlung Zangbo River is sometimes well below its long-term mean for 3–4 consecutive years. It is also possible that the flow could be depressed over a 10-year period, as in 1874–1888. Interestingly, some abnormal streamflow years in this interval were concomitant with the strong warm ENSO event of the 1877–1878 winter.

Our reconstruction provides evidence for linking the low flow of rivers draining the TP to the failure of agricultural production across the arid plains of the Indus River Valley and other Asian rivers. Major historical famines, which result from complex political and environmental factors, often occur during extreme weather events like droughts and floods (Ó Gráda, 2009). An example is the largest historical famine in Asia, which claimed over 21 million lives in China and India during 1876–1879 (Ó Gráda, 2009; Davis, 2002). That famine, caused by back-to-back shortfalls of the staple crops, was likely associated with the severe drought and water shortfalls of the reconstructed interval 1874–1888. Another example is the Bengal famine of 1943–1944, with excess mortality of three million people (Goswami, 1990), that also links to a warm ENSO event and low TP streamflow (254.5 m^3/s). Results from both observations and model simulations suggest that the frequency and severity of ENSO events will greatly increase with global warming, and more extreme El Niño events will appear under the El Niño-like background warming (Latif and Keenlyside, 2009; Xia et al., 2017; Liu et al., 2018). Thus, the risk of low-flow extremes will increase if future warm ENSO events like those of 1876–1878 recur under global warming. Meanwhile, continuous low streamflows after 2007 deserves our great attention.

5. Conclusions

We have developed a 472-year streamflow reconstruction from a ring-width standard chronology built from tree-ring cores of *Juniperus tibetica* collected from the Lhasa River Basin on the southern TP. The reconstructed record provides the information for Lhasa River streamflow during the pre-instrumental period. The streamflow reconstruction corresponds well with changes of SSTs in the Indo-Pacific Oceans, and represents regional hydroclimatic signals. We interpret the findings as further evidence, at least in part, for the influence of the ENSO and Asian summer monsoon on streamflow variation in the southern TP. While the reconstruction gives a smaller chance than the observed streamflow record that annual streamflow will fail to meet the 358.8 m^3/s baseline, or target, defined by the instrumental mean flow of the Lhasa River, severe multi-year periods of sustained low streamflow unlike any in the instrumental period occurred in the past. Recurrence of such events under global warming would have devastating effects on the entire basin, including downstream regions in India and Bangladesh. Ongoing study is providing new streamflow reconstructions for the large rivers of the southern TP. Such reconstructions will improve our understanding of the spatial-temporal changes of streamflow of the southern TP. Importantly, the development of streamflow reconstruction will be beneficial for the development of predictive models of streamflow variation, which combined with projections of fresh water demands under different socio-economics scenarios will contribute to the sustainable use of water resources in Asia.

Declaration of interest

The author declares that there is no conflict of interest.

Acknowledgments

This work was supported by the NSFC (91547115 and U1803341) and National Youth Talent Support Program. We thank the reviewers very much whose comments greatly benefited this manuscript.

Appendix A. Supplementary material

Supplementary data to this article can be found online at https://doi.org/10.1016/j.jhydrol.2019.02.054.

References

Aceituno, P., Prieto, M.D., Solari, M.E., Martínez, A., Poveda, G., Falvey, M., 2009. The 1877–1878 El Niño episode: associated impacts in South America. Clim. Change 92, 389–416.
Agafonov, L.I., Meko, D.M., Panyushkina, I.P., 2016. Reconstruction of Ob River, Russia, discharge from ring widths of floodplain trees. J. Hydrol. 543, 198–207. https://doi.org/10.1016/j.jhydrol.2016.09.031.
Bolch, T., et al., 2012. The state and fate of Himalayan glaciers. Science 336, 310–314.
Brauning, A., Griebinger, J., 2006. Late Holocene variations in Monsoon intensity in the Tibetan-Himalayan region-evidence from tree rings. J. Geol. Soc. India 68 (3), 485–493.
Chen, X., Long, D., Hong, Y., Zeng, C., Yan, D.H., 2017. Improved modeling of snow and glacier melting by a progressive two-stage calibration strategy with GRACE and multisource data: how snow and glacier meltwater contributes to the runoff of the Upper Brahmaputra River basin? Water Resour. Res. 53, 2431–2466.
Chen, F., Yuan, Y.J., Fan, Z.X., Yu, S.L., 2018. A winter precipitation reconstruction (CE 1810–2012) in the Southeastern Tibetan Plateau and its relationship to Salween River streamflow variations. Pure Appl. Geophys. https://doi.org/10.1007/s00024-018-1777-1.
Cook, E., 1985. A time series analysis approach to tree ring standardization. The University of Arizona.
Cook, E.R., Anchukaitis, K.J., Buckley, B.M., D'Arrigo, R.D., Jacoby, G.C., Wright, W.E., 2010. Asian monsoon failure and megadrought during the last millennium. Science 328 (5977). https://doi.org/10.1126/science.1185188.
Cook, E.R., Kairiukstis, L.A., 1990. Methods of dendrochronology: applications in the environmental sciences. Kluwer Academic Publishers, Dordrecht, pp. 394.
Cook, E.R., Palmer, J.G., Ahmed, M., Woodhouse, C.A., Fenwick, P., Zafar, M.U., Wahab, M., Khan, N., 2013. Five centuries of upper Indus river flow from tree rings. J. Hydrol. 486, 365–375. https://doi.org/10.1016/j.jhydrol. 2013.02.004.
Coulthard, B., Meko, D.J., Smith, D.M., 2016. Is worst-case scenario streamflow drought underestimated in British Columbia? A 332-year perspective for the south coast, derived from tree-rings. J. Hydrol. 534, 205–218.
D'Arrigo, R., et al., 2011. Reconstructed streamflow for Citarum River, Java, Indonesia: linkages to tropical climate dynamics. Clim. Dyn. 36, 451–462.
Davi, N.K., Pederson, N., Leland, C., Nachin, B., Suran, B., Jacoby, G.C., 2013. Is eastern Mongolia drying? A long-term perspective of a multidecadal trend. Water Resour. Res. 49. https://doi.org/10.1029/2012WR011834.
Davis, M., 2002. Late Victorian holocausts: El Niño Famines and the making of the third world. Verso, London.
Fan, H., He, D., 2015. Temperature and precipitation variability and its effects on streamflow in the upstream regions of the Lancang-Mekong and Nu–Salween Rivers. J. Hydrometeorol. 16 (5), 2248–2263.
Fernández, A., Muñoz, A., González-Reyes, Á., Aguilera-Betti, I., Toledo, I., Puchi, P., Sauchyn, D., Crespo, S., Frene, C., Mundo, I., González, M., Vignola, R., 2018. Dendrohydrology and water resources management in south-central Chile: lessons from the Río Imperial streamflow reconstruction. Hydrol. Earth Syst. Sci. 22, 2921–2935.
Ferrero, M.E., Villalba, R., De Membiela, M., Hidalgo, L.F., Luckman, B.H., 2015. Tree-ring based reconstruction of Río Bermejo streamflow in subtropical South America. J. Hydrol. 525, 572–584.
Fritts, H.C., 1976. Tree rings and climate. Academic Press, pp. 567.
Gao, J., He, Y., Masson-Delmotte, V., Yao, T., 2017. ENSO effects on annual variations of summer precipitation stable isotopes in Lhasa, southern Tibetan Plateau. J. Clim. https://doi.org/10.1175/JCLI-D-16-0868.1.
Gain, A.K., Wada, Y., 2014. Assessment of future water scarcity at different spatial and temporal scales of the Brahmaputra River Basin. Water Resour. Manage. 28 (4), 999–1012.
Goswami, O., 1990. The Bengal famine of 1943: re-examining the data. Indian Econ. Soc. Hist. Rev. 27 (4), 445–463.
Gou, X.H., Chen, F.H., Cook, E.R., Jacoby, G.C., Yang, M.X., Li, J., 2007. Streamflow variations of the Yellow River over the past 593 years in western China reconstructed from tree rings. Water Resour. Res. 43, W06434. https://doi.org/10.1029/2006WR005705.
Gou, X.H., Yang, T., Gao, L.L., Deng, Y., Yang, M.X., Chen, F.H., 2013. A 457-year reconstruction of precipitation in the southeastern Qinghai-Tibet Plateau, China using tree-ring records. Chin. Sci. Bull. 58 (10), 1107–1114.
Hao, Z., Zheng, J., Wu, G., Zhang, X., Ge, Q.S., 2010. 1876–1878 severe drought in North China: facts, impacts and climatic background. Chin. Sci. Bull. 55 (26), 3001–3007.
Harley, G.L., Maxwell, J.T., Larson, E., Grissino-Mayer, H.D., Henderson, J., Huffman, J., 2017. Suwannee River flow variability 1550–2005 CE reconstructed from a multispecies tree-ring network. J. Hydrol. 544, 438–451.
Harris, I., Jones, P.D., Osborn, T.J., Lister, D.H., 2014. Updated high-resolution grids of monthly climatic observations—the CRU TS3.10 Dataset. Int. J. Climatol. 34, 623–642.
Haurwitz, M.W., Brier, G.W., 1981. A critique of the superposed epoch analysismethod: its application to solar-weather relations. Monthly Weather Rev. 109, 2074–2079.
He, M., Yang, B., Bräuning, A., Wang, J., Wang, Z., 2013. Tree-ring derived millennial precipitation record for the south-central Tibetan Plateau and its possible driving mechanism. Holocene 23 (1), 36–45.
He, M., Bräuning, A., Grießinger, J., Hochreuther, P., Wernicke, J., 2018. May–June drought reconstruction over the past 821 years on the south-central Tibetan Plateau derived from tree-ring width series. Dendrochronologia 47, 48–57.
Holmes, R.L., 1983. Computer assisted quality control in tree-ring dating and measurement. Tree-Ring Bullet. 43, 69–78.
Ho, M., Lall, U., Sun, X., Cook, E.R., 2017. Multiscale temporal variability and regional patterns in 555 years of conterminous US streamflow. Water Resour. Res. 53 (4), 3047–3066.
Huang, Q., Long, D., Du, M., Zeng, C., Qiao, G., Li, X.D., Hou, A.Z., Hong, Y., 2018a. Discharge estimation in high-mountain regions with improved methods using multisource remote sensing: a case study of the Upper Brahmaputra River. Remote Sens. Environ. 219, 115–134.
Huang, Q., Long, D., Du, M., Zeng, C., Li, X., Hou, A.Z., Hong, Y., 2018b. An improved approach to monitoring Brahmaputra River water levels using retracked altimetry data. Remote Sens. Environ. 211, 112–128.
Huang, W., Feng, S., Liu, C., Chen, J., Chen, J.H., Chen, F.H., 2018c. Changes of climate regimes during the last millennium and the twenty-first century simulated by the community earth system model. Quat. Sci. Rev. 180, 42–56.
Immerzeel, W.W., Van Beek, L.P., Bierkens, M.F., 2010. Climate change will affect the Asian water towers. Science 328, 1382–1385.
Jacobs, J.W., 2002. The Mekong River commission: transboundary water resources planning and regional security. Geogra. J. 168, 354–364.
Jia, L., Zhou, S.W., 2003. The effect of Indian Ocean SST anomaly on Indian Monsoon and summer precipitation over Tibetan Plateau. Plateau Meteorol. 22 (S1), 132–137.
Kumar, R., Singh, R.D., Sharma, K.D., 2005. Water resources of India. Curr. Sci. 89, 794–811.
Lara, A., Villalba, R., Urrutia, R., 2008. A 400-year tree-ring record of the Puelo River summer–fall streamflow in the Valdivian Rainforest eco-region, Chile. Clim. Change 86, 331–356.
Lara, A., Bahamondez, A., González-Reyes, A., Muñoz, A.A., Cuq, E., Ruiz-Gómez, C., 2015. Reconstructing streamflow variation of the Baker River from tree-rings in Northern Patagonia since 1765. J. Hydrol. 529, 511–523.
Latif, M., Keenlyside, N.S., 2009. El Niño/Southern Oscillation response to global warming. Proc. Natl. Acad. Sci. 106 (49), 20578–20583.
Li, J., Xie, S.P., Cook, E.R., Huang, G., D'Arrigo, R.D., Liu, F., Ma, J., Zheng, X.T., 2011a. Interdecadal modulation of El Niño amplitude during the past millennium. Nat. Clim. Change 1, 114–118.
Li, X., Waddington, S.R., Dixon, J., Joshi, A.K., De Vicente, M.C., 2011b. The relative importance of drought and other water-related constraints for major food crops in South Asian farming systems. Food Sec. 3 (1), 19–33.
Li, F., Xu, Z., Liu, W., Zhang, Y., 2014. The impact of climate change on runoff in the Yarlung Tsangpo River basin in the Tibetan Plateau. Stoch. Env. Res. Risk Assess. 28 (3), 517–526.
Lin, X., Zhang, Y., Yao, Z., Gong, T., Wang, H., Chu, D., Liu, L.S., Zhang, F., 2008. The trend on runoff variations in the Lhasa River Basin. J. Geogr. Sci. 18 (1), 95–106.
Liu, T.C., 1999. Hydrological characteristics of Yarlungzangbo River. Acta Geogr. Sin. 54, 157–164 (in Chinese).
Liu, Y., et al., 2010. Tree-ring hydrologic reconstructions for the Heihe River watershed, western China since AD 1430. Water Res. 44, 2781–2792.
Liu, J.J., Yang, B., Qin, C., 2011. Tree-ring based annual precipitation reconstruction since AD 1480 in south central Tibet. Quat. Int. 236 (1), 75–81.
Liu, C., Huang, W., Feng, S., Chen, J.H., Zhou, A.F., 2018. Spatiotemporal variations of aridity in China during 1961–2015: decomposition and attribution. Chin. Sci. Bull. 63 (18), 1187–1199.
Long, D., Chen, X., Scanlon, B.R., Wada, Y., Hong, Y., Singh, V.P., Chen, Y., Wang, C., Han, Z., Yang, W., 2016. Have GRACE satellites overestimated groundwater depletion in the Northwest India Aquifer? Sci. Rep. 6, 24398.
Long, D., Pan, Y., Zhou, J., Chen, Y., Hou, X., Hong, Y., Scanlon, B.R., Longuevergne, L., 2017. Global analysis of spatiotemporal variability in merged total water storage changes using multiple GRACE products and global hydrological models. Remote Sens. Environ. 192, 198–216.
Mann, M.E., Lees, J.M., 1996. Robust estimation of background noise and single detection in climatic time series. Clim. Change 33, 409–445.
Maxwell, R.S., Hessl, A.E., Cook, E.R., Pederson, N., 2011. A multispecies tree ring reconstruction of Potomac River streamflow (950–2001). Water Resour. Res. 47, W05512. https://doi.org/10.1029/2010WR010019.
Meko, D.M., Woodhouse, C.A., 2005. Tree-ring footprint of joint hydrologic drought in Sacramento and Upper Colorado river basins, western USA. J. Hydrol. 308 (1–4), 196–213.
Meko, D.M., Woodhouse, C.A., Morino, K., 2012. Dendrochronology and links to streamflow. J. Hydrol. 412–413, 200–209.
Michaelsen, J., 1987. Cross-validation in statistical climate forecast models. J. Hydrol. 26, 1589–1600.
Mundo, I.A., Masiokas, M.H., Villalba, R., Morales, M.S., Neukom, R., Quesne, C.L., Urrutia, R.B., Lara, A., 2012. Multi-century tree-ring based reconstruction of the Neuquén river streamflow, northern patagonia, argentina. Clim. Past 8 (2), 815–829.
Muñoz, A.A., González-Reyes, A., Lara, A., Sauchyn, D., Christie, D., Puchi, P., Urrutia-

Jalabert, R., Toledo-Guerrero, I., Aguilera-Betti, I., Mundo, I., Sheppard, P.R., Stahle, D., Villalba, R., Szejner, P., LeQuesne, C., Vanstone, J., 2016. Streamflow variability in the Chilean Temperate-Mediterranean climate transition (35°S–42°S) during the last 400 years inferred from tree-ring records. Clim. Dyn. 47, 4051–4066.

Gráda, C.Ó., 2009. Famine. A short history. Princeton University Press, Princeton and Oxford, pp. 327.

Orr, S., Pittock, J., Chapagain, A., Dumaresq, D., 2012. Dams on the Mekong River: lost fish protein and the implications for land and water resources. Global Environ. Change 22 (4), 925–932.

Panyushkina, I.P., Meko, D.M., Macklin, M.G., Toonen, W.H.J., Mukhamdiev, N.S., Konovalov, V.G., Ashikbaev, N.A., Sagitov, A.O., 2018. Runoff variations in Lake Balkhash Basin, Central Asia, 1779 to 2015, inferred from tree rings. Clim. Dyn. https://doi.org/10.1007/s00382-018-4072-z.

Sano, M., Ramesh, R., Sheshshayee, M.S., Sukumar, R., 2012. Reconstructed June-September PDSI from tree-ring δ18O in the Nepal Himalayas. Holocene 22 (7), 809–817.

Shrestha, A., Kostaschuk, R., 2005. El Nino/Southern Oscillation (ENSO)-related variablity in mean-monthly streamflow in Nepal. J. Hydrol. 308 (1), 33–49.

Stagge, J.H., Rosenberg, D.E., DeRose, R.J., Rittenour, T.M., 2018. Monthly paleostreamflow reconstruction from annual tree-ring chronologies. J. Hydrol. 557, 791–804.

Tamkevičiūtė, M., Edvardsson, J., Pukienė, R., Taminskas, J., Stoffel, M., Corona, C., Kibirkštis, G., 2018. Scots pine (*Pinus sylvestris* L.) based reconstruction of 130 years of water table fluctuations in a peatland and its relevance for moisture variability assessments. J. Hydrol. 558, 509–519.

Torrence, C., Compo, G.P., 1998. A practical guide to wavelet analysis. Bull. Am. Meteorol. Soc. 79, 61–78.

Trinh, L.T., Duong, C.C., Van Der Steen, P., Lens, P.N., 2013. Exploring the potential for wastewater reuse in agriculture as a climate change adaptation measure for Can Tho City, Vietnam. Agric. Water Manage. 128, 43–54.

Urrutia, R.B., Lara, A., Villalba, R., Christie, D.A., Le Quesne, C., Cuq, A., 2011. Multicentury tree ring reconstruction of annual streamflow for the Maule River watershed in south central Chile. Water Resour. Res. 47, W06527. https://doi.org/10.1029/2010WR009562.

Wigley, T., Briffa, K.R., Jones, P.D., 1984. On the average value of correlated time series, with applications in dendroclimatology and hydrometeorology. J. Clim. Appl. Meteorol. 23, 201–213.

Woodhouse, C.A., Stahle, D.W., Villanueva Díaz, J., 2012. Rio Grande and Rio Conchos water supply variability over the past 500 years. Climate Res. 51 (2), 147–158. https://doi.org/10.3354/cr01059.

Xia, Y., Sun, X., Yan, Y., Feng, W., Huang, F., Yang, X.Q., 2017. Change of ENSO characteristics in response to global warming. Chin. Sci. Bull. 62 (16), 1738–1751 (In Chinese).

Xue, Y., Wang, Y., 2005. Highly controversial hydropower development in western China. The China environmental year book, pp. 63–88.

Yang, B., Qin, C., Shi, F., Sonechkin, D.M., 2012. Tree ring-based annual streamflow reconstruction for the Heihe River in arid northwestern China from AD 575 and its implications for water resource management. Holocene 22 (7), 773–784.

Yang, B., Qin, C., Wang, J., He, M., Melvin, T.M., Osborn, T.J., Briffa, K.R., 2014. A 3500-year tree-ring record of annual precipitation on the north-eastern Tibetan Plateau. Proc. Natl. Acad. Sci. 111, 2903–2908. https://doi.org/10.1073/pnas.1319238111.

Yao, T., et al., 2012. Different glacier status with atmospheric circulations in Tibetan Plateau and surroundings. Nat. Clim. Change 2 (9), 663–667.

Yao, T., et al., 2013. A review of climatic controls on δ18O in precipitation over the Tibetan Plateau: observations and simulations. Rev. Geophys. 51, 525–548. https://doi.org/10.1002/rog.20023.

Yi, S., Song, C., Wang, Q., Wang, L., Heki, K., Sun, W., 2017. The potential of GRACE gravimetry to detect the heavy rainfall-induced impoundment of a small reservoir in the upper Yellow River. Water Resour. Res. 53 (8), 6562–6578.

Zhang, Q.B., Evans, M.N., Lyu, L., 2015. Moisture dipole over the Tibetan Plateau during the past five and a half centuries. Nat. Commun. 6, 8062.

Zhang, Q., Xu, C.Y., Jiang, T., Wu, Y., 2007. Possible influence of ENSO on annual maximum streamflow of the Yangtze River, China. J. Hydrol. 333 (2), 265–274.

Zhou, S., Jia, J., Du, J., 2001. Response of the summer precipitation over the Tibetan Plateau to ENSO events. J. Nanjing Inst. Meteorol. 24, 570–575 (In Chinese).